

One-year measurements of surface heat budget on the ablation zone of Antizana Glacier 15, Ecuadorian Andes

Vincent Favier, Patrick Wagnon, Jean-Philippe Chazarin, Luis Maisincho, Anne Coudrain

▶ **To cite this version:**

Vincent Favier, Patrick Wagnon, Jean-Philippe Chazarin, Luis Maisincho, Anne Coudrain. One-year measurements of surface heat budget on the ablation zone of Antizana Glacier 15, Ecuadorian Andes. Journal of Geophysical Research: Atmospheres, 2004, D18105 [15 p.]. 10.1029/2003JD004359 . ird-01223136

HAL Id: ird-01223136
https://ird.hal.science/ird-01223136

Submitted on 2 Nov 2015

HAL is a multi-disciplinary open access archive for the deposit and dissemination of scientific research documents, whether they are published or not. The documents may come from teaching and research institutions in France or abroad, or from public or private research centers.

L'archive ouverte pluridisciplinaire **HAL**, est destinée au dépôt et à la diffusion de documents scientifiques de niveau recherche, publiés ou non, émanant des établissements d'enseignement et de recherche français ou étrangers, des laboratoires publics ou privés.

One-year measurements of surface heat budget on the ablation zone of Antizana Glacier 15, Ecuadorian Andes

Vincent Favier,[1] Patrick Wagnon,[2] Jean-Philippe Chazarin,[1] Luis Maisincho,[3] and Anne Coudrain[4]

Received 17 November 2003; revised 4 April 2004; accepted 15 April 2004; published 17 September 2004.

[1] Meteorological variables were recorded (14 March 2002 to 14 March 2003) at 4890 m above sea level (asl) on the Antizana Glacier 15 (0.71 km^2; 0°28′S, 78°09′W) in the tropical Andes of Ecuador (inner tropics). These variables were used to compute the annual cycle of the local surface energy balance (SEB). The four radiative fluxes were directly measured, and the turbulent fluxes were calculated using the bulk aerodynamic approach, calibrating the roughness length by direct sublimation measurements. The meteorological conditions are relatively homogeneous throughout the year (air temperature and air humidity). There is a slight seasonality in precipitation with a more humid period between February and June. During June-September, wind velocity shows high values and is responsible for intense turbulent fluxes that cause reduction of melting. Considering the SEB over the whole year, it is dominated by net radiation, and albedo variations govern melting. During the period under consideration the net short-wave radiation S (123 W m^{-2}) and the sensible turbulent heat flux H (21 W m^{-2}) were energy sources at the glacier surface, whereas the net long-wave radiation L (-39 W m^{-2}) and the latent turbulent heat flux LE (-27 W m^{-2}) represented heat sinks. Since the O°C isotherm-glacier intersection always oscillates through the ablation zone and considering that the phase of precipitation depends on temperature, temperature indirectly controls the albedo values and thus the melting rates. This control is of major interest in understanding glacier response to climate change in the Ecuadorian Andes, which is related to global warming and ENSO variability. *INDEX TERMS:* 1827 Hydrology: Glaciology (1863); 1863 Hydrology: Snow and ice (1827); 3307 Meteorology and Atmospheric Dynamics: Boundary layer processes; 3374 Meteorology and Atmospheric Dynamics: Tropical meteorology; *KEYWORDS:* inner tropics' glacier, energy balance, melting, albedo, temperature

Citation: Favier, V., P. Wagnon, J.-P. Chazarin, L. Maisincho, and A. Coudrain (2004), One-year measurements of surface heat budget on the ablation zone of Antizana Glacier 15, Ecuadorian Andes, *J. Geophys. Res.*, *109*, D18105, doi:10.1029/2003JD004359.

1. Introduction

[2] Mountain glaciers respond rapidly to climatic change. Hence a general scientific effort aims at better understanding the relation between glacier evolution and the different aspects of changes in climate [e.g., *Kuhn*, 1981; *Oerlemans*, 2001; *Kaser and Osmaston*, 2002]. Tropical glaciers are particularly sensitive to the effects of global warming [e.g., *Hastenrath and Kruss*, 1992], to El Niño events [e.g., *Kaser et al.*, 1990; *Wagnon et al.*, 2001; *Francou et al.*, 2004] as well as to changes in the moisture regime [e.g., *Mölg et al.*, 2003; *Francou et al.*, 2003]. Establishing the physical relationship between glacier and climate needs to study the SEB. The present study is therefore a new effort to follow up the energy balance of the world's glaciers over long-time periods (months to years), as already conducted for instance in the Sierra Nevada [*Marks and Dozier*, 1992], in Antarctica [*Bintanja et al.*, 1997], in the Alps [e.g., *Oerlemans and Klok*, 2002; *Klok and Oerlemans*, 2002], and in the outer tropics [*Wagnon et al.*, 1999].

[3] Our study addresses the Antizana Glacier 15, which is located in the inner tropics [*Kaser and Osmaston*, 2002]. This equatorial region of South America is particularly interesting because (1) it is characterized by a slight seasonality in precipitation compared to the pronounced dry and wet seasons observed in the outer tropics and because (2) the glacier is proximal to the Pacific Ocean, source of El Niño events that may influence noticeably the temperature [*Vuille et al.*, 2000] and slightly the precipitations [*Vuille et al.*, 2000].

[4] The text below first describes the measurement program and the local climatic conditions. Presented next are

[1]Maison des Sciences de l'Eau, Institut de Recherche pour le Développment (IRD), Montpellier, France.
[2]Laboratoire de Glaciologie et Géophysique de l'Environnement (LGGE), Institut de Recherche pour le Développment (IRD), Saint Martin d'Hères, France.
[3]Instituto Nacional de Meteorologia e Hidrologia (INAMHI), Quito, Ecuador.
[4]UMR Hydrosciences, Maison des Sciences de l'Eau, Montpellier, France.

Copyright 2004 by the American Geophysical Union.
0148-0227/04/2003JD004359$09.00

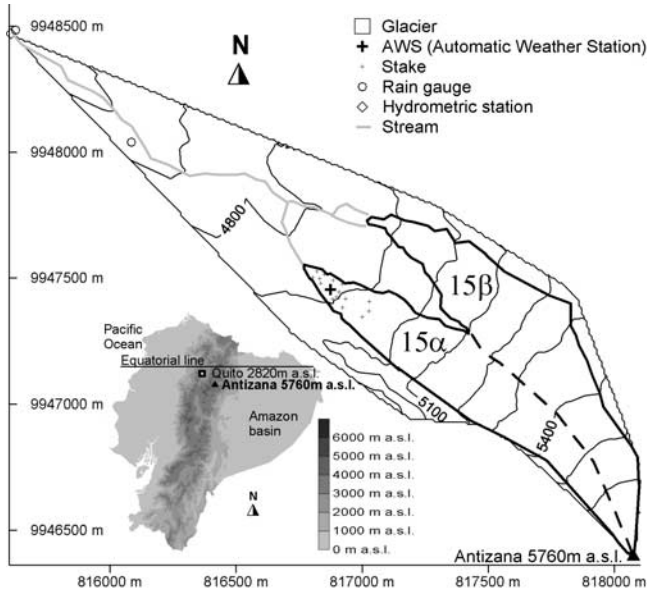


Figure 1. Orientation map of Antizana Glacier 15 showing location of monitoring equipment. Projection is on UTM zone 17. Lower plot is a physical map of Ecuador.

the methods used to compute all the terms of the SEB. Finally, results are exposed and then discussed to select the main variables that control the melting process on Antizana Glacier 15.

2. Location and Measurement Program

[5] Antizana Glacier 15 (0.71 km^2, 0°28′S, 78°09′W), is located 40 km east of Quito (the capital of Ecuador). This glacier, made up of two similarly oriented side-by-side tongues called glaciers 15 α and glacier 15 β (Figure 1), extends from 5760 m asl down to 4840 m asl. It stands on the NW slope of Antizana volcano, one of the main volcanic range of the eastern cordillera of Ecuador (Figure 1). It is strongly exposed to the incoming airflows from the Amazon basin [*Francou et al.*, 2000].

[6] Apart from the monthly precipitation amounts recorded at 4650 m asl from January 1995 to March 2003, we use in this paper the following data acquired between 14 March 2002 and 14 March 2003: (1) daily precipitation from an automatic precipitation gauge located at 4550 m asl, (2) half-hourly meteorological data sets recorded by a Campbell (UK) automatic weather station (AWS) located at 4890 m asl, (3) monthly measurements from 15 ablation stakes, and (4) sporadic measurements of daily melting and sublimation. The AWS has been installed in September 1998, at the foot of the ablation zone of glacier 15α (4890 m asl), however the CM3 and CG3 radiative sensors (i.e., a CNR1 net radiometer) were installed only on 14 March 2002 (Table 1). The location of the AWS makes the weather station representative of the surface condition of the lower half of the ablation zone (equilibrium line altitude at approximately 5030 m asl). The weather station is set up on the glacier near its axis, on a relatively flat surface. Routine visits are made approximately every 10 days to check that it is functioning properly. Table 1 lists the sensors that the station is equipped with, their specifications, and their respective height in relation to the glacier surface. All sensors were calibrated during the year before the study period. The weather station records the half-hourly mean of the measurements taken every 15 s, except for the wind direction that corresponds to a single measurement every 30 min. The sun reaches the weather station at approximately 0800 local time (LT) and sets at approximately 1800 LT. At the measurement site, the main obstructions are located from NE to SE and the value of the related mask is 5%.

[7] Two periods remain without data because the weather station's power battery discharged, one lasted from 7 April to 15 April and the other one from 2 May to 8 May. For the first period, it was possible to reconstruct most of the data (temperature, humidity, wind speed, and wind direction) thanks to a mobile AWS that was placed on the glacier roughly 20 m away from the weather station. Indeed, comparisons of these data with the ones from the weather station, when available, are good. However, the mobile AWS was equipped with two Kipp and Zonen SP-Lite pyranometers (precision given by the manufacturer: ±3%)

Table 1. List of Equipment: Sensors and Their Specifications and Rain Gauge Characteristics[a]

Element[b]	Sensor Type	Height,[c] cm	Accuracy According to the Manufacturer
Air temperature, °C	Vaisala HMP 45, aspirated[d]	30 and 180	±0.2°C
Relative humidity, %	Vaisala HMP 45, aspirated[d]	30 and 180	±2%
Wind speed, m s^{-1}	Young 05103	30 and 180	±0.3 m s^{-1}
Wind direction, deg	Young 05103	30 and 180	±3 deg
Incident short-wave radiation,W m^{-2}	Kipp&Zonen CM3, 0.305 < λ < 2.8 μm	85	±3%
Reflected short-wave radiation, W m^{-2}	Kipp&Zonen CM3, 0.305 < λ < 2.8 μm	85	±3%
Incoming long-wave radiation, W m^{-2}	Kipp&Zonen CG3, 5 < λ < 50 μm	85	±3%
Outgoing long-wave radiation, W m^{-2}	Kipp&Zonen CG3, 5 < λ < 50 μm	85	±3%
Element	Sensor Type	Altitude	Characteristics and Accuracy
Monthly mean values of precipitation	Manual measurements	4650 m asl	opening: 2000 cm^2 height: 150 cm ± 5 mm
Daily mean values of precipitation	Automatic Hobo Rain Gauge[e]	4550 m asl	opening: 200 cm^2 height: 100 cm

[a]Sensors are installed at 4890 m asl.
[b]Quantities are recorded as half-hourly means over 15-s time intervals except for wind direction, which are instantaneous values every 30 min.
[c]Heights are variable but known with reasonable accuracy thanks to manual measurements every 10 days.
[d]To prevent measurement errors due to radiation, Vaisala hygrothermometers are adequately shielded and artificially ventilated.
[e]Tipping bucket recording rain gauge measured precipitation at 0.21 mm.

Table 2. List of Multiday Field Trips and Estimation of the Roughness Length z_0 by Application of the Bulk Aerodynamic Approach Between 14 March 2002 and 14 March 2003

Field Trip	Beginning	End	Roughness Length, mm	Number of Lysimeters
1	14 March 2002	19 March 2002	2.2	5
2	26 April 2002	02 May 2002	0.017	3
3	21 May 2002	25 May 2002	4.6	5
4	23 July 2002	31 July 2002	2.7	3
5	22 Aug. 2002	26 Aug. 2002	2.3	2
6	26 Sept. 2002	30 Sept. 2002	3.0	2
7	30 Nov. 2002	4 Dec. 2002	3.5	4
8	29 Jan. 2003	3 Feb. 2003	2.2	4
Roughness mean (without trip 2)			2.9	

and a Kipp and Zonen NR-Lite radiometer (precision: ±3%); we therefore do not have access to both incoming and outgoing long-wave radiation for this period.

[8] In addition meteorological observations (wind speed and wind orientation, type of weather, cloudiness, type of clouds) and surface conditions analyses were carried out during field trips lasting 5–10 days (Table 2). These field campaigns allowed to carry out direct sublimation measurements using "poor man's lysimeters" that consist of translucent plastic boxes filled with snow or ice and inserted so as to reproduce the surface condition of the glacier as faithfully as possible [*Hastenrath*, 1978]. The weight of these boxes was measured at regular intervals with a precision of ±1 g, approximately ±1 W m^{-2}). We took care not to consider the measurements disturbed by precipitation in the boxes. During these field trips, daily melting measurements were also carried out by the use of "melting boxes" similar to those described by *Wagnon et al.* [1999].

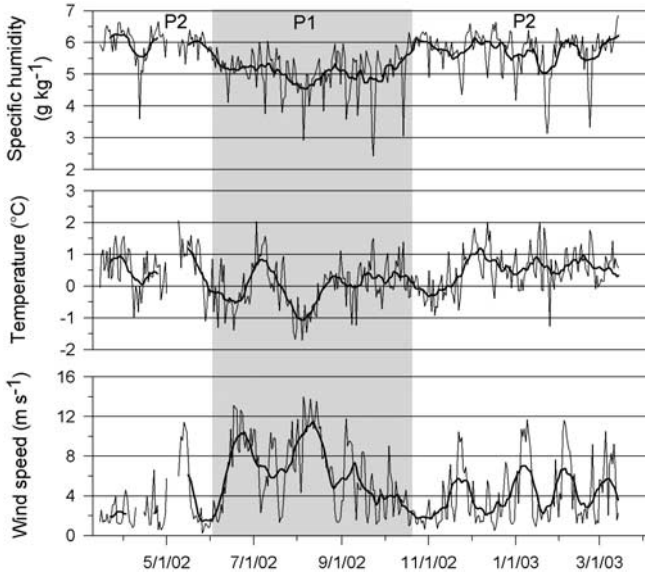


Figure 2. Daily means of ventilated temperature, specific humidity, and wind speed on Antizana Glacier 15, 4890 m asl, between 14 March 2002 and 14 March 2003. Thick lines are the 15-day running means. The shaded and white areas refer to two distinct periods of the year, P1 (1 June 2002 to 15 October 2002) and P2 (14 March 2002 to 31 May 2002 and 16 October 2002 to 14 March 2003).

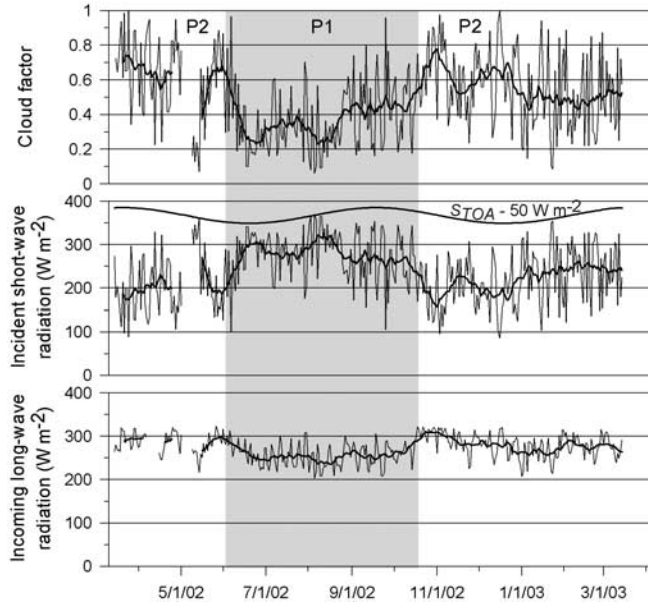


Figure 3. Daily means of cloudiness, incident short-wave radiation, and incoming long-wave radiation on Antizana Glacier 15, 4890 m asl, between 14 March 2002 and 14 March 2003. Also shown is the top of atmosphere solar irradiance reduced by 50 W m^{-2}. Thick lines are the 15-day running means. The shaded and white areas refer to two distinct periods of the year, P1 (1 June 2002 to 15 October 2002) and P2 P2 (14 March 2002 to 31 May 2002 and 16 October 2002 to 14 March 2003).

3. Climatic Conditions

[9] The inner tropics are characterized by a thermically homogenous atmosphere with slightly variable humidity throughout the year [e.g., *Hastenrath*, 1991, p. 25; *Kaser*, 2001]. That is confirmed by the measurements of specific humidity, air temperature and wind speed performed between 14 March 2002 and 14 March 2003 at 4890 m asl on Antizana Glacier 15 (Figure 2). The standard deviation of daily measurements is 0.7 g kg^{-1} for the specific humidity and 0.7°C for the temperature. This confirms that in the Andean region of Ecuador, temperature and humidity variations are not large enough to characterize a pronounced seasonal regime. The average temperature is 0.3°C for the cycle studied, in good accordance with the altitude of 4950 m asl for the 0°C isotherm previously published [*Schwerdtfeger*, 1976, p. 176]. Two other variables also show very little variations, the day length (only a few minutes) and the top of the atmosphere solar irradiance (S_{TOA} in Figure 3).

[10] Cloud cover is a good indicator of the radiation contribution. Periods of high cloud cover result in a decrease in the incident short-wave radiation contribution partly compensated by the increased incoming long-wave radiation. This transfer influences the nyctemeral (daily) distribution of the energy provided to the surface. From 630 LT to 1830 LT, diurnal values of the cloudiness also called

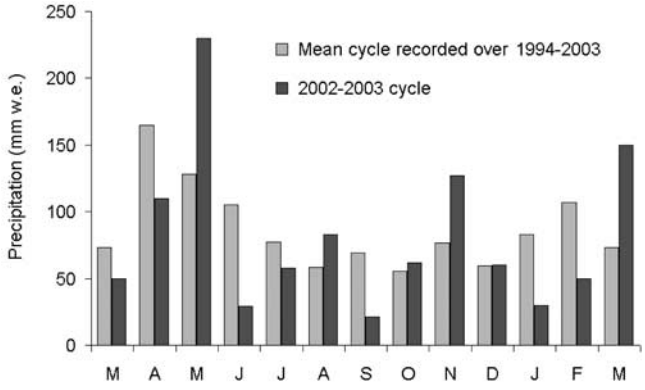


Figure 4. Monthly precipitation on Antizana at 4650 m asl from March 2002 to March 2003 and monthly means of precipitation recorded over 1994–2003.

the cloud factor n (nondimensional), can be calculated by comparing the incident short-wave radiation ($S\downarrow$) (in W m^{-2}) to the theoretical values of the top of atmosphere solar irradiance S_{TOA} (in W m^{-2}) using the following expression [*Sicart*, 2002, p. 253]:

$$n = 1.3 - 1.4(S\downarrow / S_{TOA}) \quad (1)$$

S_{TOA} is obtained by considering the solar constant equal to 1368 W/m^2. *Bourges* [1985] provides the solar declination values. Equation (1) is in agreement with the atmospheric attenuation observed for clear days at the site (attenuation of approximately 10%, or -50 W m^{-2}, for the daily mean values) and for days of maximal cloud cover (approximately 80%, or 340 W m^{-2}). The cloud factor (n) shows high values (more than 0.6) during the two periods with higher precipitation amount (March to May and November, Figures 3 and 4). The periods of maximal top of atmosphere solar irradiance were those of minimal contribution of short-wave radiation at the surface of the glacier.

[11] The wind plays a central role in local climatology. Wind speed is anticorrelated with cloud cover (in daily means, r = -0.66, n = 354). Substantial downhill air advection limits condensation phenomena that generates clouds and precipitation [e.g., *Barry*, 1992, p. 115]. The heaviest precipitations occur when the wind velocity is weak to moderate (mean daily wind speed is less than 5 m s^{-1}). Cloudiness and specific humidity are correlated (r = 0.60, n = 359). Consequently, as low humidity and strong wind accelerate sublimation, windy days are favorable to substantial sublimation on Antizana.

[12] At higher levels, easterlies with varying meridional components prevail over the Equatorial Americas throughout the year [*Hastenrath*, 1981, p. 12]. During boreal summer, intensified easterlies extend into the midtroposphere in the equatorial belt. Then, in the high Andes of Ecuador, the wind at 500 hPa is very strong and the weather is generally clear [*Hastenrath*, 1981, p. 13]. On Antizana volcano, the wind is the strongest in JJAS (Figure 2, average daily velocities are often greater than 10 m s^{-1}), which is in agreement with the more pronounced easterly zonal circulation. The main orientation of the wind corresponds to the orientation of the overall forcing but also of the katabatic winds (Figure 5). At night, high-elevation surfaces experience radiative cooling and katabatic winds are intensified [e.g., *Martin*, 1975; *Van den Broeke*, 1997; *Oerlemans*, 1998; *Oerlemans and Grisogono*, 2002]. Diurnal thermal winds [e.g., *Van den Broeke*, 1997; *Oerlemans*, 1998] are weak, thus winds from the west are more frequent between 1400 and 1700 LT (heightened convective phenomena on glacier edges during the day). However, wind speed maximum has never been observed within the first 5 m above the surface (not shown), and thus easterlies usually prevail over katabatic winds.

[13] The Antizana precipitation regime is complex (Figure 4). Substantial precipitation is observed all the year-round, the lowest monthly mean value is 56 mm (October, mean value for the period between 1995 to 2003). The heaviest precipitations were observed in April, May, and November 2002 and in March 2003. Considering the available data set between 1995 and 2003, there is always a period with heavy precipitation between February and June, although the beginning of this wet season is extremely variable. Generally another month between September and November shows high amount of precipitation (i.e., November in 2002). These features reflect the different origins of precipitation at the Antizana. First, Antizana receives precipitation from the Amazon basin. The eastern slopes of the Andes are the first obstacles encountered by air masses coming from the east and pushed by the trade winds from the Atlantic [*Vuille et al.*, 2000], creating an ascent of the air and an adiabatic cooling leading to heavy precipitations [*Schwerdtfeger*, 1976, p. 154]. Second, the site is located in a border zone with the inter-Andean plateau whose precipitation regime is noticeably different: "the Andes represent a powerful divide for the lower tropospheric flow" [*Hastenrath*, 1981, p. 14]. Thus, on Antizana, the

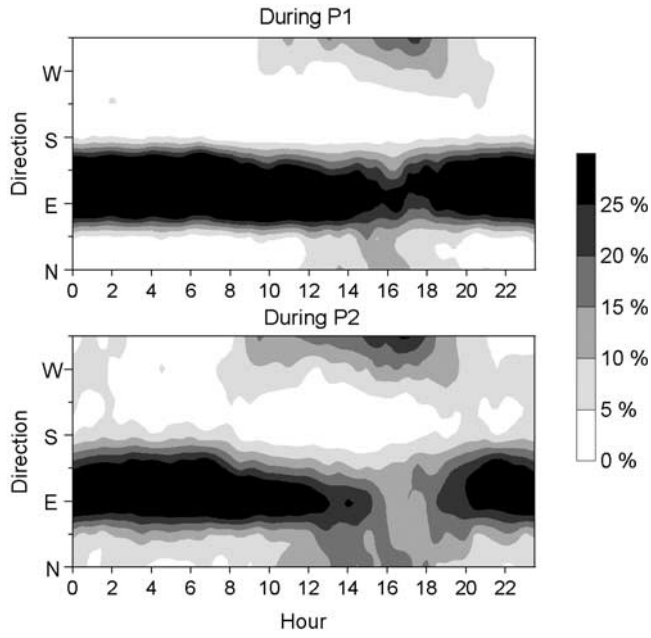


Figure 5. Frequency of wind direction distribution during P1 (1 June 2002 to 15 October 2002) and P2 (14 March 2002 to 31 May 2002 and 16 October 2002 to 14 March 2003).

Table 3. Mean Values of Meteorological and SEB Variables During P1, During P2, Difference Between P1 and P2, Annual Mean, and Standard Deviation[a]

Element	P1	P2	Difference (P1–P2)	Annual Mean	Standard Deviation
R_h, %	76	84	−8	81	11
q, g kg^{-1}	5.0	5.8	−0.8	**5.5**	0.7
T, °C	0.0	0.5	−0.5	**0.3**	0.7
u, m s^{-1}	6.6	3.6	3.0	**4.8**	3.5
S_{TOA}, W m^{-2}	418	417	1	417	13
Cloudiness	0.37	0.59	−0.22	0.50	0.23
$S\downarrow$, W m^{-2}	278	215	63	239	68
$S\uparrow$, W m^{-2}	148	96	52	116	51
Albedo	0.53	0.44	0.09	0.49	0.18
$L\downarrow$, W m^{-2}	256	282	−26	272	29
$L\uparrow$, W m^{-2}	309	313	−3	311	3
T_s, °C	−1.8	−1.1	−0.7	−1.4	0.7
L, W m^{-2}	−53	−31	−22	**−39**	27
S, W m^{-2}	130	119	10	**123**	57
R, W m^{-2}	77	89	−12	84	46
z_0, mm	2.9	2.9	-	2.9	-
LE, W m^{-2}	−47	−14	−32	**−27**	31
H, W m^{-2}	30	16	15	**21**	19
$LE + H$, W m^{-2}	−16	1	−18	−6	17
$(LE + H)/R$, %	21	2	-	**7**	-
$R + LE + H$, W m^{-2}	60	90	−30	78	49
Precipitation, mm	275	695	-	**970**	-
Rain, mm	30	225	-	255	-
Snow, mm w.e.	245	470	-	715	-
Melting, mm w.e.	2120	5280	-	**7400**	-
Corrected melting,[b] mm w.e.	∼2300	∼4050	-	**∼6350**	-
Sublimation, mm w.e.	200	100	-	**300**	-

[a]Symbols represent relative humidity (R_h), specific humidity (q), temperature (T), wind speed (u), extraterrestrial irradiance (S_{TOA}), incident and reflected short-wave radiations (S↓ and S↑, respectively), incoming and outgoing long-wave radiation (L↓ and L↑, respectively), surface temperature (T_s), net short-wave and long-wave radiations (S and L, respectively), net all-wave radiation (R), roughness length (z_0), turbulent latent and sensible heat fluxes (LE and H, respectively), and sum of turbulent heat fluxes (LE+H).

[b]Geometrical corrections of $S\downarrow$ are made considering the coarse assumption that incident short-wave radiation is purely direct, and that slope angle is 18° (mean glacier slope).

precipitation regime of the Amazon regions (a single maximum between June and July and a minimum in February [*Schwerdtfeger*, 1976, p. 155]) is mixed with the inter-Andean valley regime (with two wet seasons in February-May and October-November) [*Vuille et al.*, 2000].

[14] Given the close relation between wind speed seasonality and the intra-annual variations of moisture, the year may be divided into two main periods, the delineations of which are defined after Figure 2. The characteristics of every period are summarized below and in Table 3. (1) The first period (P1) is from 1 June to 15 October. With mean values of wind speed, specific humidity, cloud factor and temperature of 6.6 m s^{-1}, 5.0 g kg^{-1}, 0.37 and 0.0°C, respectively, P1 is a very windy but also moderately dry and cold period. P1 corresponds also to a season of reduced precipitation. (2) The second period (P2) is from 16 October to 31 May. Compared to P1, the mean wind speed is almost reduced by half (3.6 m s^{-1}), the average cloud factor is sharply enhanced (n = 0.59), while temperature and humidity are slightly higher (0.5°C and 5.8 g kg^{-1} respectively). Consequently, P2 is a period of low wind but enhanced cloud cover and thus precipitation.

[15] The cycle studied is close to the mean values recorded since 1995 for the total precipitation. For the year 2002, the amount is 985 mm at 4650 m asl (970 mm, for the studied cycle), which is slightly lower than the annual mean (1055 mm for the 8 years measured; standard deviation = 228 mm). The wettest month for the 2002–2003 cycle is May, although it is April for the 1995–2002 period. The investigated cycle shows three marked minima: June 2002, September 2002 and January 2003. It is also slightly warmer (0.3°C) than the mean value since September 1998 (0.1°C; standard deviation of daily means = 0.8°C, for 1187 complete days). Finally, *Francou et al.* [2004] discuss the representativeness of the 2002–2003 studied cycle more precisely.

4. Surface Energy Balance Study

[16] A unit volume of glacier is defined from the surface to a depth where there are no significant heat fluxes. On this volume, for a unit of time, and assuming a lack of horizontal energy transfers, the surface energy balance equation is written as follows, where the fluxes toward the surface are positive [e.g., *Oke*, 1987, p. 90]:

$$R + H + LE + G + P = \Delta Q_M + \Delta Q_S = \Delta Q \qquad (2)$$

R is the net all-wave radiation, H is the turbulent sensible heat flux, LE is the turbulent latent heat flux. The conductive heat flux in the snow/ice G can be disregarded as the glacier is isothermal. The heat advected by precipitation P is insignificant compared to the other terms [e.g., *Wagnon et al.*, 1999]. ΔQ_M is the latent heat storage change due to melting and freezing and ΔQ_S is the net convergence or divergence of sensible heat fluxes within the volume. The change of the energy ΔQ is stored in the volume or utilized in the melting process. If the very top layers of the glacier have a temperature below 0°C, then ΔQ corresponds to a temperature change within the surface layers. If these layers are at 0°C, then ΔQ is available for the melting process.

4.1. Net All-Wave Radiation

[17] The net radiation is the balance of the incident and reflected short-wave radiations and the incoming and outgoing long-wave radiations:

$$R = S\downarrow - S\uparrow + L\downarrow - L\uparrow = S\downarrow (1 - \alpha) + L\downarrow - L\uparrow \qquad (3)$$

where $S\downarrow$ is the incident short-wave radiation, $S\uparrow$ is the reflected short-wave radiation ($S = S\downarrow - S\uparrow$ is the net short-wave radiation), α is the short-wave albedo of the snow/ice surface, $L\downarrow$ is the incoming long-wave radiation, and $L\uparrow$ is the outgoing long-wave radiation ($L = L\downarrow - L\uparrow$ is the net long-wave radiation).

[18] In the present study, the four terms of the surface radiative balance (second term of equation (3)) were measured on the field site by a Kipp and Zonen net radiometer (model CNR1), composed of two CM3 pyranometers (short-waves: $0.305 < \lambda < 2.8$ μm) and two CG3 pyrgeometers (long-waves: $5 < \lambda < 50$ μm).

[19] Although *Obleitner and de Wolde* [1999] suggested to apply a systematic correction to the measurements of long-wave radiations in relation to incident solar radiation, we decided not to apply this correction because surface temperature derived from outgoing long-wave radiation was in a better agreement with observed surface temperature

during field trips without this correction than with it. This is probably due to the fact that wind speed is usually strong enough to maintain a sufficient natural ventilation and thus to prevent the sensor from radiative heating. In some cases the value of $S\uparrow$ was greater than $S\downarrow$*0.9. Considering that the maximum realistic value of albedo is 0.9 and the measurement of $S\uparrow$ was probably altered by the surface inclination or by snowfalls covering the upper pyranometer, in these cases, a systematic correction was applied to $S\downarrow$: $S\downarrow = S\uparrow/0.9$. Such corrections concerned only the early morning values or the periods with heavy snowfalls and they do not affect the monthly and annual values of short-wave radiation.

4.2. Turbulent Fluxes

4.2.1. Bulk Method

[20] The turbulent heat fluxes were calculated using the bulk aerodynamic approach, including stability correction. This method is usually used for practical purposes because it approximates the turbulent heat fluxes from one level of measurement [*Arck and Scherer*, 2002]. Moreover, *Denby and Greuell* [2000] showed that this method is usually more appropriate over snow surfaces and with the presence of low-level katabatic wind speed maximum. *Arck and Scherer* [2002] also showed that this method yields the best correlation to the eddy-covariance measurements, particularly as long as air temperature is negative. In this approach, a constant gradient is assumed between the level of measurement and surface and thus surface values have to be evaluated. The stability of the surface layer is described by the bulk Richardson number Ri_b, which relates the relative effects of buoyancy to mechanical forces [e.g., *Brutsaert*, 1982; *Moore*, 1983; *Oke*, 1987]:

$$Ri_b = \frac{g\dfrac{\Delta T}{\Delta z}}{T\left(\dfrac{\Delta u}{\Delta z}\right)^2} = \frac{g(T - T_s)(z - z_{0m})}{Tu^2} \tag{4}$$

where T and u are the mean values of air temperature (in K) and horizontal wind speed (in m s^{-1}) respectively at the level of measurement z. g is the acceleration of gravity (g = 9.81 m s^{-2}), T_s is the surface temperature (in K) and z_{0m} is the surface roughness length for momentum (in m). By definition, z_{0m} is the fictitious height where, taking into account a semilogarithmic profile, the horizontal component of the wind speed is zero, $u(z_{0m}) = 0$. Ri_b is positive in a stable atmosphere. Assuming that local gradients of mean horizontal wind speed u, mean temperature T and mean specific humidity q are equal to the finite differences between the measurement level and the surface, it is possible to give analytical expressions for the turbulent fluxes [e.g., *Oke*, 1987]:

$$\tau = \rho u^{*2} = \rho\frac{(ku)^2}{\left(\ln\dfrac{z}{z_{0m}}\right)^2}(\Phi_m)^{-2} \qquad \left(\text{in kg m}^{-1}\,\text{s}^{-2}\right) \tag{5}$$

$$H = \rho\frac{C_p k^2 u(T - T_s)}{\left(\ln\dfrac{z}{z_{0m}}\right)\left(\ln\dfrac{z}{z_{0t}}\right)}(\Phi_m\Phi_v)^{-1} \qquad \left(\text{in W m}^{-2}\right) \tag{6}$$

$$LE = \rho\frac{L_s k^2 u(q - q_s)}{\left(\ln\dfrac{z}{z_{0m}}\right)\left(\ln\dfrac{z}{z_{0q}}\right)}(\Phi_m\Phi_v)^{-1} \qquad \left(\text{in W m}^{-2}\right) \tag{7}$$

where q_s is the mean specific humidity at the surface (in g kg^{-1}), ρ = 0.72 kg m^{-3} is the air density at 4890 m asl (570 hPa), C_P is the specific heat capacity for air at constant pressure ($C_p = C_{pd}(1 + 0.84q)$ with C_{pd} = 1005 J kg^{-1} K^{-1}, the specific heat capacity for dry air at constant pressure), L_s is the latent heat of sublimation of snow or ice (L_s = 2.834 10^6 J kg^{-1}), and k is the von Karman constant (k = 0.4). τ is the surface stress and u* is the characteristic scale of velocity (in m s^{-1}), also called the friction velocity. z_{0m}, z_{0T} and z_{0q} are the surface roughness lengths for momentum, temperature and humidity, respectively. In order to compute turbulent fluxes (equations (5), (6), and (7)), it is assumed, as already mentioned, that the horizontal component of the wind speed is zero at z_{0m}, it is also assumed that the air temperature is equal to that of snow/ice surface at z_{0T}, and finally that the air is saturated with respect to snow/ice surface temperature at z_{0q}. This last assumption helps to calculate the surface specific humidity q_s. To apply the bulk aerodynamic approach for the measurements on Antizana Glacier 15, the surface temperature T_s was derived from the outgoing long-wave radiation $L\uparrow$ using the Stefan-Boltzmann equation assuming that the emissivity of the snow is unity, $L\uparrow = \sigma T_s^4$ with $\sigma = 5.67\ 10^{-8}$ W m^{-2} K^{-4}. A change in emissivity from 1 to 0.99 leads to very small differences in long-wave radiation compared to sensor uncertainty (from 315.6 W m^{-2} to 312.5 W m^{-2} for a melting snow surface (0°C)).

[21] The nondimensional stability functions for momentum (Φ_m), heat (Φ_h) and moisture (Φ_v) can be expressed in terms of Ri_b:

$$\text{For } Ri_b \text{ positive (stable)}: \quad (\Phi_m\Phi_h)^{-1} = (\Phi_m\Phi_v)^{-1} = (1 - 5Ri_b)^2 \tag{8}$$

$$\text{For } Ri_b \text{ negative (unstable)}: \quad (\Phi_m\Phi_h)^{-1} = (\Phi_m\Phi_v)^{-1} = (1 - 16Ri_b)^{0.75} \tag{9}$$

[22] The bulk method was applied between the surface and the level of measurement of T and q. Since u was not measured exactly at the same elevation to prevent perturbations from the AWS mast, the wind speed was recalculated at the level of T and q assuming that the vertical wind speed profile is logarithmic (neutral conditions): $u = \frac{u^*}{k}\ln(z/z_{0m})$ with u* defined by equation (5).

[23] We also define the characteristic scales of potential temperature and of specific humidity by:

$$\theta^* = H/\left(\rho C_p u^*\right) \qquad (\text{in K}) \tag{10}$$

$$q^* = LE/(\rho L_s u^*) \qquad \left(\text{in g kg}^{-1}\right) \tag{11}$$

[24] A detailed study of the temperature profiles in the first meter of the atmosphere showed that a warm-layer very occasionally exists. However, this feature on the Antizana Glacier 15 is much weaker than already observed on other glaciers [e.g., *De la Casinière*, 1974; *Halberstam and Schieldge*, 1981; *Male and Granger*, 1981; *Meesters et al.*, 1997; *Wagnon et al.*, 1999], and the influence on turbulent fluxes computation can be disregarded. Moreover, we did not observe any wind speed maxima within the 5 m

above the snow/ice surface. Hence it can be assumed that the measurements of temperature and wind speed were made within the dynamic sublayer, and thus that the assumption of semilogarithmic profiles is justified.

4.2.2. Roughness Lengths

[25] As in the work of *Wagnon et al.* [1999], the surface roughness lengths were all chosen equal, $z_{0m} = z_{0T} = z_{0q} = z_0$, and were used as calibration parameters. Indeed, z_0 is calibrated in order to fit the mean calculated sublimation (obtained from *LE* derived from the bulk method) over the period with direct measurements to the mean measured sublimation on the same period obtained by averaging the values of the lysimeters. Except *King and Anderson* [1994], who found z_{0T}, $z_{0q} \gg z_{0m}$ over an Antarctic ice shelf in winter, most of the authors and theoretical work suggest that z_{0T} and z_{0q} are 1 or 2 orders of magnitude lower than z_{0m} [e.g., *Ambach*, 1986; *Andreas*, 1987; *Morris*, 1989; *Munro*, 1989; *Hock and Holmgren*, 1996; *Meesters et al.*, 1997]. Values from the literature are highly dependent on local conditions. Given the wide range of values, we chose to retain a single roughness length for the three variables. Since these parameters are calibrated on direct measurements, taking different values for z_{0m}, z_{0T} and z_{0q} would have changed the values of these parameters but not the final results of the turbulent fluxes.

[26] For the eight field trips of several days conducted on Antizana Glacier 15 in 2002 and 2003, the calibrated roughness length values range between 2.2 mm and 4.6 mm and one value is remarkably small (0.017 mm) (Table 2). This small value corresponds to a 6-day field trip characterized by low wind (2.4 m s^{-1}, mean value between 26 April 1200 LT and 2 May 1000 LT) and fresh snow at the glacier surface which induces small turbulent fluxes and thus very reduced sublimation (0.05 mm w.e. day^{-1}, mean value between 26 April and 2 May). Since applying our calibration method over insignificant values obviously leads to a bad estimate of z_0, this value is imprecise and probably underestimates the actual roughness. The presence of such fresh snow occurs only few weeks a year. We thus assumed that the roughness lengths measured during the seven other missions are representative of the surface condition during the cycle studied. Computing the daily sublimation values with different calibrated z_0 values or with a constant value corresponding to the average one (z_0 = 2.9 mm (Figure 6)) of the seven field trips show quite similar results. Henceforth, z_0 will always be considered equal to 2.9 mm.

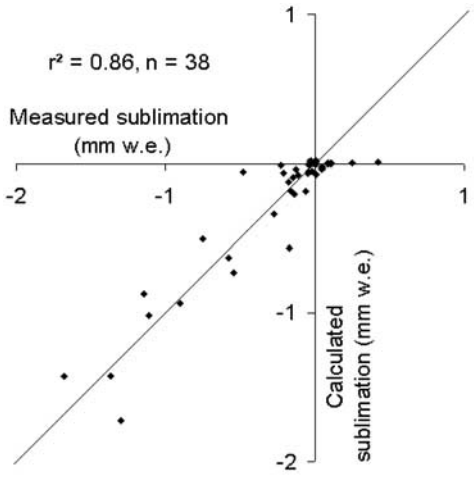


Figure 6. Comparison of computed and measured daily sublimation values during field trips with a constant roughness length value z_0 = 2.9 mm. Also shown is the 1:1 line.

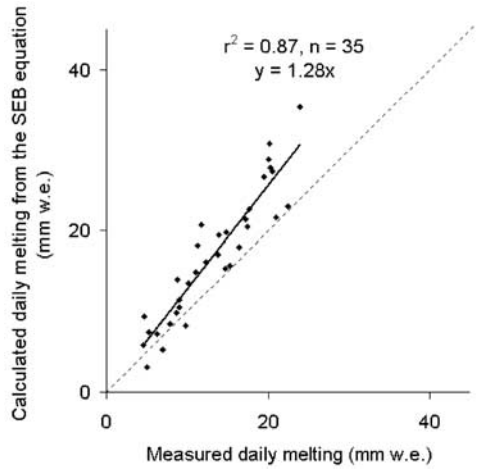


Figure 7. Comparison of daily melting calculated from the SEB equation and measured by melting boxes during field trips. Also shown is the 1:1 line (dashed line) and the regression line (solid line).

4.3. Comparison Between Calculated and Measured Local Daily Melting

[27] In this case study, the melting occurs every day and the sensible heat storage ΔQ_S is zero for a daily time step. The melting boxes allow measuring exclusively the melting over one day. Hence measurements from melting boxes can be compared to the daily value of calculated melting term, ΔQ_M. The comparison shows good agreement (Figure 7, r^2 = 0.87, n = 35). It is interesting to note that when the turbulent fluxes (*H* and *LE*) are disregarded, the correlation is much worse and the computed melting may overestimate the measured values of more than 100% for several points. For these specific points, daily sublimation is as high as 3 mm water equivalent (w.e.) ($LE = -100$ W m^{-2}). Consequently, turbulent heat fluxes cannot be neglected.

[28] Considering the 35 couples of the calculated daily melting and the measured ones show that calculated values exceed the mean value of the melting boxes of about 30%. However, this difference is relatively small with regard to the accuracy of the daily melting measured by the boxes where the snow/ice surface and density do not precisely reproduce the natural conditions (cryoconite holes, stirring up of the impurities).

4.4. Comparison Between Calculated and Measured Monthly Ablation

[29] The computed ablation (melting + sublimation) based on the SEB equation was compared with the monthly balance from 15 stakes in the ablation zone (Figure 1). For March 2002, mass balance value is for 15 days only. For May 2002, the computed ablation was obtained by extending the mean of available values over the entire month. For March 2003, the ablation was computed from AWS measurements from 1 March 2003 to 1 April 2003

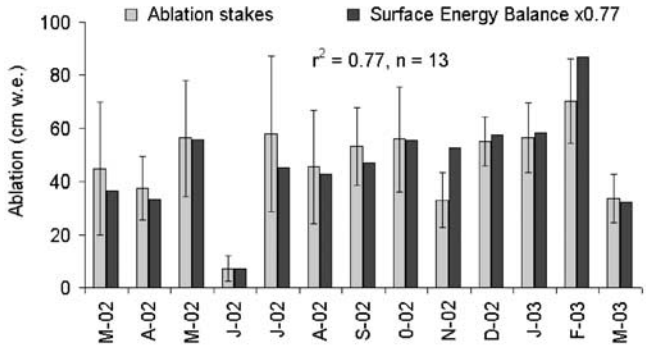


Figure 8. Monthly energy balance on Antizana Glacier 15, 4890 m asl, and monthly means of ablation measurements on 15 glaciological stakes between 4850 and 5000 m asl, from March 2002 to March 2003. The SEB values presented here are divided by a factor of 1.3. Also shown are the standard deviations of ablation measurements on the 15 glaciological stakes.

and compared to the monthly value of ablation obtained with mass balance measurements (the AWS recordings from 15 March 2003 to 1 April 2003 were not integrated into the rest of the study to retain a cycle of 365 days, but the values do not change the interpretation of the results).

[30] The correlation between computed ablation and glaciological measurements is strong (r^2 = 0.79, n = 13). However, the computed ablation is about 1.3 times higher than the measured one (Figure 8). Neglecting the correction of long-wave radiation measurements due to sensor's heating up as a result of the substantial incident radiation $S\downarrow$ might explain part of this difference. However, an explanation of this systematic overestimation is more likely found in the effects of slope angle and aspect (orientation) of the surface on solar radiation income. Since net radiation sensor is placed parallel to the horizon, geometrical corrections of $S\downarrow$ [*Barry*, 1992, pp. 76–79] are necessary to compute local melting. As a coarse assumption, considering that incident short-wave radiation is purely direct, the correction for a maximal slope angle of 18 degrees (i.e., the average glacier slope), leads to a better agreement between calculated and measured local ablation (r^2 = 0.86, slope = 1) (Table 3). With this maximal correction, on one hand, the incident short-wave radiation impinging on the glacier surface would increase from April to August. On the other hand, a slight decrease would occur during December-January. However, the lack of knowledge of exact diffuse and direct components of the incident solar radiation and of accurate slope angle and orientation at the AWS site prevents us from giving a rigorous and systematic correction. At this stage of knowledge, we choose not to take into account this correction. Anyway, the temporal variations are similar with or without correction and this 30% difference does not alter the discussion and conclusions drawn from the analysis of the main variables of the melting processes.

5. Results

5.1. Analysis of the Two Meteorological Periods

[31] During the P1 period (1 June 2002 to 15 October 2002) characterized by stronger and more frequent easterlies even during afternoons (Figure 5), the computed energy available for melting (from equation (1)) is 60 W m^{-2} compared to 90 W m^{-2} during the complementary period P2 (Table 3). Indeed strong wind, a driver of turbulence, was during P1 a source of significant turbulent heat fluxes that reduced the available energy for melting. Considering the whole cycle (Figure 9), LE and H show similar evolution with high absolute values in August ($LE = -64$ W m^{-2} corresponding to a total of 60 mm w.e. of sublimation). For August, the overall turbulent fluxes ($LE + H = -21$ W m^{-2}) represent 30% of R (73 W m^{-2}). Hence for hydrological modeling, the turbulent fluxes cannot be ignored at least during periods with strong wind.

[32] Between P1 and P2, analysis of the different SEB terms shows that the turbulent fluxes difference (-18 W m^{-2}) is responsible for 60% of the drop in melting at 30 W m^{-2}. The diminution of net radiation (-12 W m^{-2}) explains the remaining 40%. The explanation of the latter decrease is found in the albedo (+0.09 between P2 and P1). Indeed, the decrease in $L\downarrow$ (-26 W m^{-2}) (related to the decrease in cloudiness (-0.22)) is largely compensated by the increase in $S\downarrow$ (+63 W m^{-2}) showing that conditions encountered on the glacier are far from the ones of the radiation paradox as described by *Ambach* [1974]. So albedo appears to be a central variable of the energy balance because its variations control net radiation. The energy balance is, indeed, very highly correlated with the surface albedo (r^2 = 0.79, n = 13 (in monthly values)) (Figure 9).

5.2. Daily Cycles of the SEB Variables

5.2.1. Short-Wave Radiation

[33] Figure 10 illustrates the daily evolution of the albedo, cloudiness and radiative terms. In the morning, incident radiation followed the extraterrestrial radiation (S_{TOA}) but with a delay (not shown): because of the glacier's aspect (northwest slope) the weather station is located in the peak's shadow zone. The very high cloud factor observed in the morning is a measurement artifact caused by the weather station being in shadow. As soon as the weather station comes out of the shadow, radiation increases abruptly and follows the cycle of S_{TOA}.

[34] Even though the sun rises at approximately 615 LT all yearlong, the station received the first sun rays slightly earlier during P1 (730 versus 800 LT): the mask is less facing north. Thus the radiation curves for the two periods follow each other but with a slight delay.

[35] During P1, the attenuation of extraterrestrial radiation was lower because of the lower cloud cover. $S\downarrow$ was higher, particularly in the afternoon (Figure 10). Cloudiness, low in the morning, progressively increased from 1400 to 1700 LT ($n_{max} \sim 0.5$) because convective clouds that formed during the day gathered at that time. During P2, the increase in the cloud factor followed the same trend but it began earlier (1000 LT) and was much more pronounced ($n_{max} \sim 0.8$).

[36] The means of $S\downarrow$ at 1600 and 1630 LT of P1 were slightly affected by the shadow of the mast: the albedo and cloud factor curves show a slight peak (Figure 10). For the days concerned, this measurement error contributed less than 0.5% of the daily contribution of $S\downarrow$. Here also we chose not to systematically correct the affected data. Finally,

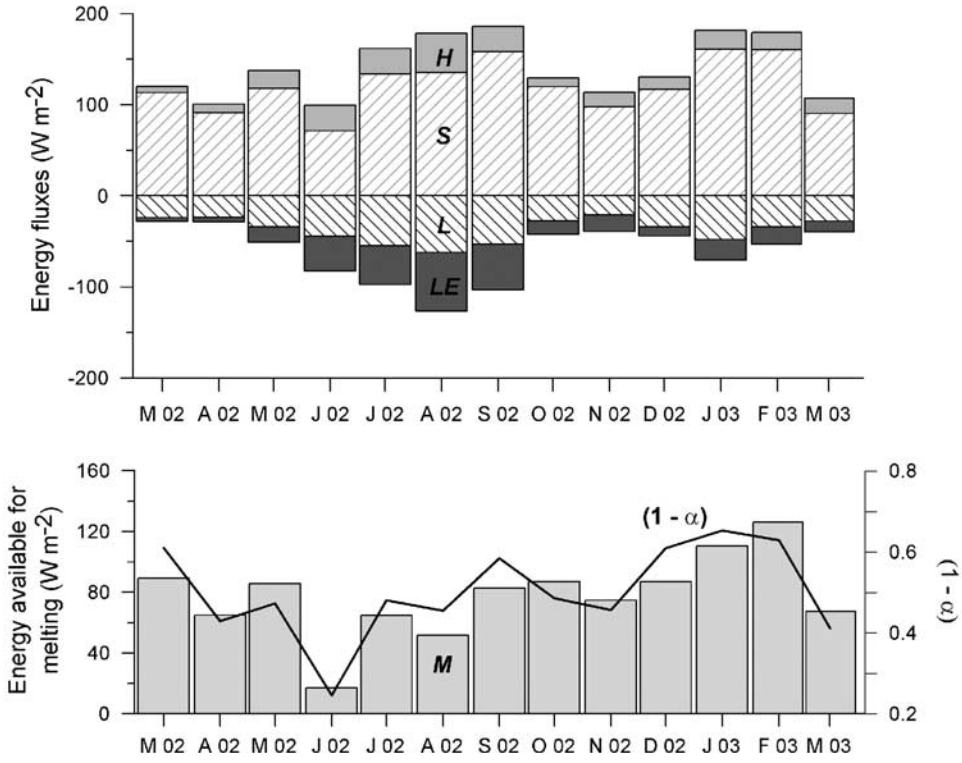


Figure 9. Monthly means of net short-wave radiation (S), net long-wave radiations (L), turbulent sensible and latent heat fluxes (H and LE, respectively), melting (M) and 1 − albedo (1 - α) from March 2002 to March 2003.

after 1700 LT cloudiness declined. This is not a measurement artifact, but a trend confirmed by field observations.

[37] The reflected radiation followed the variations of $S\downarrow$, but the lower the albedo the more it was attenuated (Figure 10). As a result of the increase in $S\downarrow$ and α, $S\uparrow$ was much higher during P1 (148 versus 96 W m^{-2}). In the morning the values were disturbed by the screen effect of the mountain because the weather station was in shadow. As soon as the sun came out, the albedo values decreased progressively until 1230 LT. The albedo was at its lowest between 1230 and 1330 LT and then increased more sharply in the afternoon. Several reasons can explain this more pronounced trend: the slope aspect [*Sicart et al.*, 2001], the presence of cryoconite holes observed in the field when the ice was not covered with snow, the increase in cloudiness during the day (more pronounced attenuation of radiation in the near infrared and absorption spectrum of the snow [*Warren*, 1982]) and the more frequent snowfalls during the afternoon. This increase was similar for both periods, making it more probable that the effects of the slope and site exposure dominate in this phenomenon.

5.2.2. Surface Temperature T_s and Long-Wave Radiation

[38] Observation of the values of T_s (equivalent to observing $L\uparrow$) showed that the glacier was in more pronounced refreezing conditions during P1 (Figure 10): (1) melting started later, 1100 LT instead of 1000 LT (T_s = 0°C); (2) melting conditions were observed until 1600 LT instead of 1700–1800 LT; (3) when melting stopped, progressively, refreezing and then nighttime cooling were observed. The minimum temperature, reached at 630 LT in both cases, was 1°C lower for the first period (−3.5°C versus −2.6°C).

[39] $L\downarrow$ showed a marked daily cycle, with a similar trend for both periods: nighttime values were lower by 30 W m^{-2} than daytime values. The increase followed the increase in cloudiness, air temperature and humidity, with a slight delay (3–4 hours) compared to the sun's cycle. Over the entire day, the lowest cloudiness during P1 resulted in lower values of 26 W m^{-2} on average.

5.2.3. Net Radiation Balance

[40] P1 nocturnal net radiation was lower (−60 W m^{-2} versus −40 W m^{-2}) and was part of a more pronounced refreezing and a slight delay in melting during the day

Figure 10. Mean diurnal cycle of meteorological and SEB variables during P1 (shaded lines) and during P2 (solid lines). Thick lines are the surface characteristics that are the surface specific humidity (q_s), the surface temperature (T_s), the surface albedo (α). Thin lines are the wind speed (u), the air specific humidity (q), the air temperature (T), the diurnal cloud factor (n), the incident and the reflected short-wave radiations ($S\downarrow$ and $S\uparrow$, respectively), the incoming and the outgoing long-wave radiation ($L\downarrow$ and $L\uparrow$, respectively), the turbulent sensible heat flux (H), the net all-wave radiation (R), and the sum of turbulent heat fluxes ($LE + H$). Lines with dots represent the turbulent latent heat flux (LE) and the energy available for the melting (M).

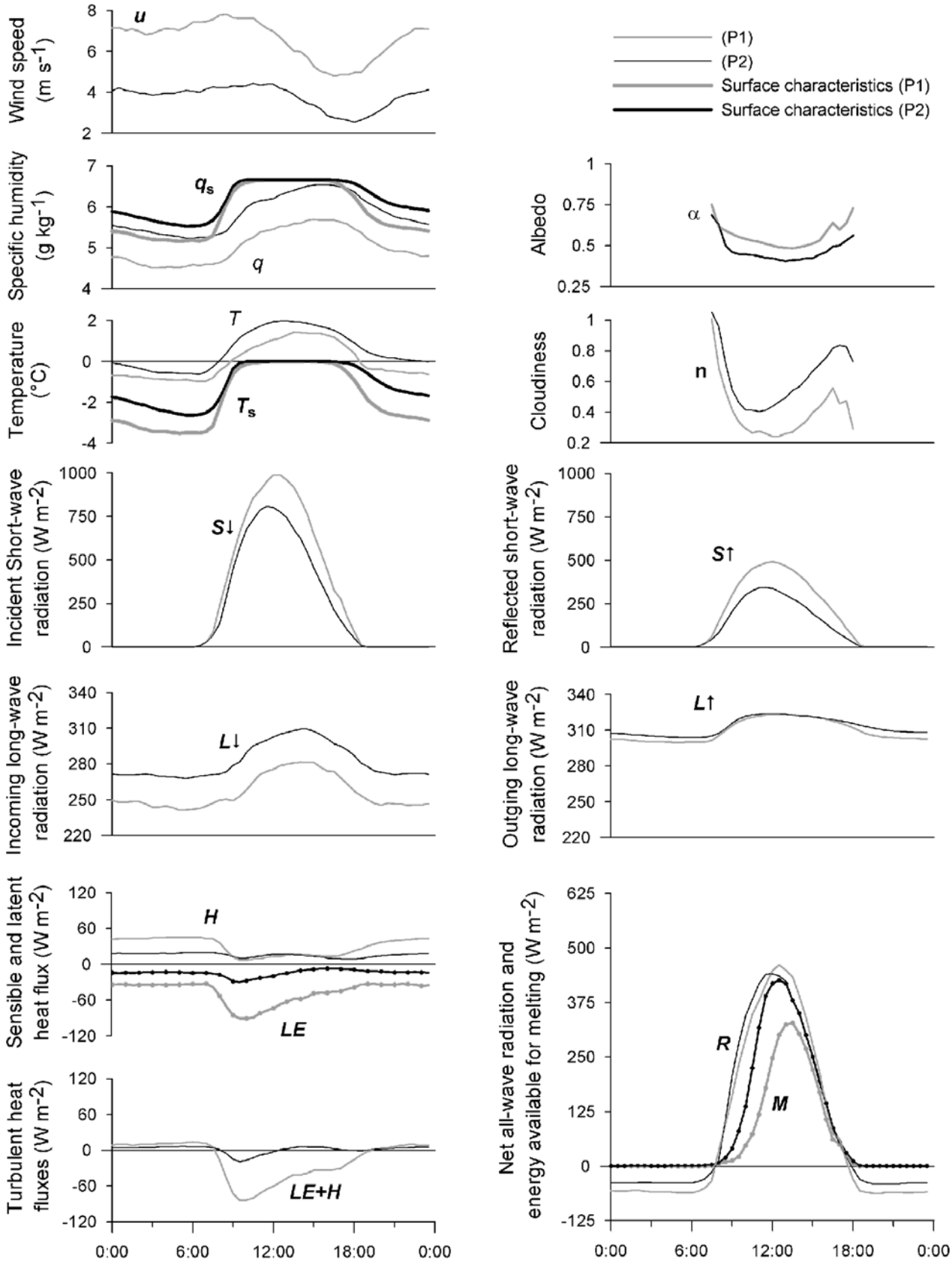

Wind speed (m s-1)
u
Specific humidity (g kg-1)
qs
q
Temperature (°C)
T
Ts
Incident Short-wave radiation (W m-2)
S↓
Incoming long-wave radiation (W m-2)
L↓
Sensible and latent heat flux (W m-2)
H
LE
Turbulent heat fluxes (W m-2)
LE+H
(P1)
(P2)
Surface characteristics (P1)
Surface characteristics (P2)
Albedo
α
Cloudiness
n
Reflected short-wave radiation (W m-2)
S↑
Outging long-wave radiation (W m-2)
L↑
Net all-wave radiation and energy available for melting (W m-2)
R
M
0:00
6:00
12:00
18:00
0:00

Figure 10

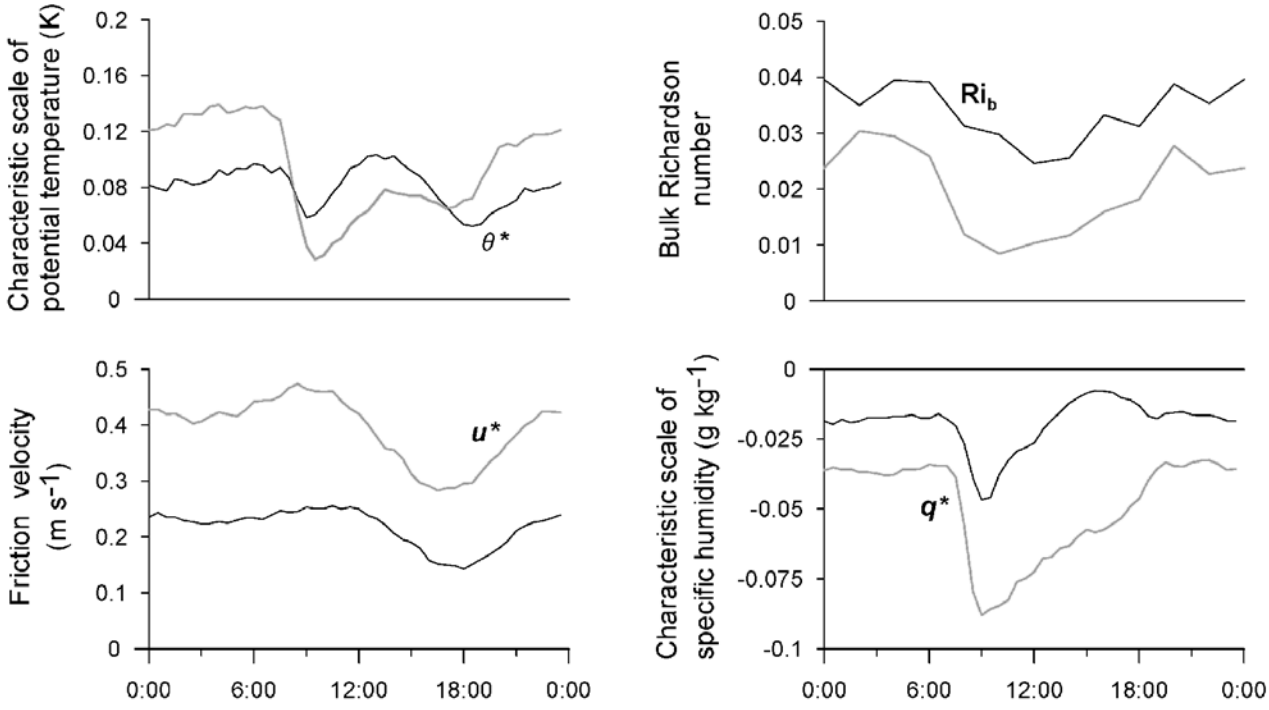


Figure 11. Mean diurnal cycle of friction velocity (u^*), and of characteristic scales of potential temperature (θ^*) and specific humidity (q^*) during P1 (shaded lines) and during P2 (solid lines). Also shown is the mean diurnal cycle of the bulk Richardson number (Ri_b) during P1 (shaded line) and P2 (solid line).

(Figure 10), in relation to the cloudiness difference between the two periods. For these diurnal values, both cycles were nearly identical: the effects of the albedo difference compensated the effects of cloudiness. The maximum was moved forward 1 hour (1230 LT instead 1130 LT), proof of the earlier arrival of cloud cover in the morning. The amplitude during P1 was slightly higher (approximately 40 W m^{-2}).

5.2.4. Turbulent Fluxes

[41] LE, H, and $LE + H$ maintained an identical trend for the two periods. However, the magnitude was very different (Figure 10). At night, the air was cooled little by little by the colder surface. Conditions were stable ($Ri_b \sim 0.03$) (Figure 11). The high level of stratification is confirmed by the slight nighttime increase in u^* (Figure 11 and equation (5)): the katabatic wind became more pronounced. The temperature gradient resulted in an energy contribution at the surface as $H > 0$ [e.g., *Oerlemans*, 1998]. The easterlies came down the glacier's slopes, heating up rapidly but carrying little humidity (foehn effect [e.g., *Barry*, 1992]): the snow/ice surface sublimated. Consequently, LE and H were opposed and of equal amplitude and the turbulent fluxes were balanced during the night ($LE + H \approx 0$ W m^{-2}). Despite a strong wind, the high stability resulted in relatively weak fluxes ($H \approx -LE \approx$ 40 W m^{-2} and 10 W m^{-2}, respectively, for P1 and P2).

[42] At sunrise, short-wave radiation resulted in rapid heating of the snow and ice. Surface and air temperatures were very close and θ^* (equation (10) and Figure 11) dropped sharply to nearly zero: H tended toward zero. Parallel to temperature, the saturation humidity at the surface rose quickly, while air humidity was still low (the air masses were not yet loaded with humidity): $|q^*|$ (equation (11) and Figure 11) rose. The high values of $|q^*|$ were associated with a decrease in air stability. This decrease is sharper during P1 ($Ri_b \sim 0$), sublimation was therefore maximal. $|LE + H|$ created a substantial loss of energy for the surface of the snow.

[43] Little by little, the surface temperature rose to reach the melting temperature of the snow. The rise in surface temperature then ceased and the air, warming up, returned to more stable conditions (Ri_b is increased again). Thus $|q^*|$ decreased and θ^* increased (heightened stability): $LE + H$ was balanced little by little.

[44] The increase in Ri_b should be viewed parallel with the decrease in u^* during the day: the wind turned west (ascendance) and became less intense. In the evening, the stable conditions of the night were restored as soon as the Sun set. Between the two periods of the year, θ^* evolved very little. In addition, the difference in amplitude of $LE + H$ is related to the higher values of u^* and q^* for P1. The drop in Ri_b (less marked stability), however, is essentially related to the greater intensity of the wind (nearly factor two) during P1.

5.2.5. Melting

[45] Melting begins with a slight delay compared to R increase in the morning. The average refreezing amounts of the night affect the melting until the beginning of the afternoon. However, the diurnal melting is noticeably more delayed during P1. The stronger radiative cooling during the night and the more important diurnal heat sinks of turbulent heat fluxes explain this important difference.

5.3. Using SEB Measurements for Mass Balance Model Specifications

[46] With the SEB measurements in the Ecuadorian Andes available from this study, it is possible to specify

the parameters used in mass balance modeling as described by *Kaser* [2001] or *Kuhn* [1981]. "The man who doesn't like clouds has no business coming to Ecuador" [*Michaux*, 1928, p. 34]. The frequent bad weather that characterizes Ecuador usually leads to the idea that cloud cover is heavy and precipitations are large. Actually, Antizana's precipitation accumulations are moderate. The average accumulation since 1995 amounts to 1055 mm w.e. year^{-1}, lower than the value of 1600 mm w.e. year^{-1} proposed by *Kaser* [2001]. The contribution of $S\downarrow$ = 239 W m^{-2} (Table 3) (20.4 MJ m^{-2} d^{-1}) is in agreement with the value proposed by *Kuhn* [1981] and *Kaser* [2001]. However, the approximation of the emissivity of the atmosphere ε_{atm} = 0.7 [*Kuhn*, 1981; *Kaser*, 2001]) is significantly smaller than the actual value determined by the present study (considering that $L\downarrow$ = 272 W m^{-2} and T_a = 0.3°C, we obtain ε_{atm} = 0.86). This difference corresponds to 10°C, but temperatures of 10°C have never been observed on Antizana.

[47] The turbulent flux values also provide interesting aspects. Sublimation was generally ignored because of high levels of humidity [e.g., *Kuhn*, 1981]. This study shows that sublimation amounts to 300 mm w.e. for the 2002–2003 cycle (LE = −27 W m^{-2}, Table 3) which is far from negligible, as an energy sink, compared to melting (7400 mm w.e., or 78 W m^{-2}). *Kaser* [2001] already suspected this point and incorporated it in his model by a factor "f," which describes the partition of available energy between energy and melting. This study confirms that f = 20% is a minimum to adopt in mass balance modeling. H partially compensates for the losses due to sublimation. The sensible heat flux value makes it possible to calculate a heat transfer coefficient, β. With H value of 21 W m^{-2} for a mean air temperature (T_a) of 0.3°C and a snow/ice surface temperature (T_s) of −1.4°C, the value of β is approximately of 1.1 MJ m^{-2} d^{-1} °C^{-1}. This is comparable to values available in the literature (e.g., β = 1.7 MJ m^{-2} d^{-1} °C^{-1} [*Kuhn*, 1981; *Kaser*, 2001]). Field measurements allow to compute all the SEB terms, and give the opportunity to be more accurate in exploring the terms responsible for mass balance variability.

6. Discussion

[48] In this section, variations of the melting, actually of the albedo, are discussed in comparison with meteorological forcings. The significance of temperature and precipitation frequency in establishing snow cover at the glacier surface is shown as the main factor controlling albedo variations and therefore melting variations. Here, precipitation separation into rain and snow is based on a subjective criterion of limit temperature: we assume that rain occurs only if T > 0.5°C. Although *Klok and Oerlemans* [2002] used a threshold of 1.5°C to separate liquid and solid precipitation, 0.5°C reproduces the actual conditions with good accuracy, compared to field observations (Figure 12).

[49] In section 5.1, albedo appears as a central variable in melting. There is a close relation, at a daily time step, between the albedo and the net radiation balance (r = −0.80, n = 359). The successive increases in albedo go hand in hand with an abrupt drop in the short-wave radiation balance (r = −0.79, n = 359). Variations in the short-wave radiation balance (S) are of much greater amplitude than those of the net long-wave radiation (Figure 12). Thus S controls the melting evolution.

[50] Moreover, Figure 12 shows the importance of snowfalls in attenuating the melting processes: (1) After rainfall events, albedo remains low ($\alpha \leq 0.6$) and quickly decreases to less than 0.4. Then, melting shows high values. For example, pronounced rain period around 15 May, or the rain event of 28 November, or at the beginning of March 2003 did not establish a new snow mantle: albedo remained near 0.3. (2) After snowfalls, albedo increases sharply ($\alpha \geq 0.7$) and melting decreases noticeably. However, only substantial snowfalls durably impede melting. For example, the small snowfalls at the end of October 2002 had weak effects on albedo and on the melting. On the contrary, important snowfall on 30 July led to a substantial decline in melting until 20 August. (3) After heavy snowfalls, albedo climbs to 0.9. However, the progressive metamorphism of snow involves a progressive decline in albedo to values close to 0.7 (for example, after important snowfalls at the ends of May and July 2002). This decline is accompanied by light melting with little variations. Abruptly, albedo values drop to 0.3 with the appearance of ice, and melting increases sharply. This phenomenon is described by classic albedo modeling [e.g., *U.S. Army Corps of Engineers*, 1956; *Brun et al.*, 1989, 1992; *Oerlemans and Knap*, 1998; *Hock*, 1998]. As a consequence, after long periods of weak accumulated precipitations, snow disappears and melting rates inexorably recover (for example, during July, September, and December 2002 or January 2003). (4) Between 1 June and 15 October (P1 period), melting was limited due to intense turbulent fluxes (20% of the net radiation values during this period). Moreover, strong turbulent fluxes during June and August are partly responsible for a slow down of albedo degradation velocity involving a longer persistence of snow cover. Wind speed is then an important variable to explain limited melt during P1.

[51] Precipitation and temperature during the main precipitation period (between February and June) are therefore crucial for the annual glaciological mass balance. For the cycle studied, the main snowfall events occurred late in the year (at the end of May) and after a long warm period, involving noticeable mass balance deficit as shown by 2002–2003 local ablation measured by glaciological stakes (−6650 mm w.e. (Table 3)). Significant snowfall in February and April would have clearly reduced the ensuing melting. Long periods without snowfall result in a significant increase in melting. Likewise the occurrence of considerable precipitations in September, instead of November, would have limited the melting of the following months. Finally, early starting and longer windy period would have involved higher sublimation sink and longer persistence of snow cover on the glacier surface: the limitation of the windy period is not totally rigid. Occurrence of slight winds during P1 would have involved stronger melt.

[52] The high sensitivity of Ecuadorian glaciers to climate is strongly linked to the absence of seasonality in temperatures. The 0°C isotherm consistently oscillates through the ablation zone of the glacier, and the smallest variation in air temperatures can influence the melting

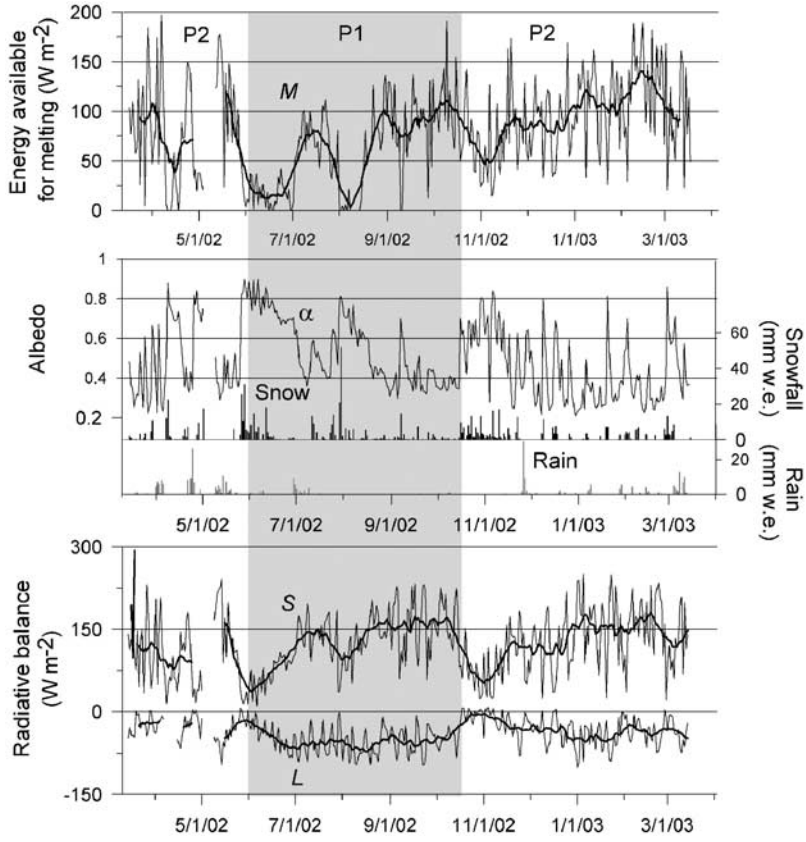


Figure 12. Daily means of the short-wave radiative balance (S), of the long-wave radiative balance (L), of the melting (M) of the snow/ice and of the albedo (α) from 14 March 2002 to 14 March 2003. Also shown are the precipitation amounts with snow (solid bars) and rain (shaded bars) delineated on the base of thermal threshold ($T > 0.5$°C). Thick lines are the 15-day running means. The shaded and white areas refer to two distinct periods of the year, P1 (1 June 2002 to 15 October 2002) and P2 (14 March 2002 to 31 May 2002 and 16 October 2002 to 14 March 2003).

processes by determining the phase of precipitation in the ablation zone. This justifies that relation between altitude of the equilibrium line and the 0°C level line is a decisive parameter of glaciers' sensitivity to climatic variations [e.g., *Kaser*, 2001].

[53] This study gives an interesting additional information to study the glacier shrinkage in the Andes of Ecuador where near-surface temperature appears to be strongly affected by climate variability. The link between temperature anomalies in the equatorial atmosphere and the sea surface temperature anomalies [*Vuille et al.*, 2000], along with near-surface temperature increase of the last decades [e.g., *Diaz and Graham*, 1996; *Gaffen et al.*, 2000; *Vuille and Bradley*, 2000] are consistent with important glacier retreat observed on Antizana Glacier 15 [*Francou et al.*, 2000]. The control of temperature on the phase of precipitations is one of a dominant factors explaining ENSO impact on Antizana Glacier 15 [*Francou et al.*, 2004].

7. Summary and Conclusion

[54] Despite the absence of a pronounced seasonality in temperature and humidity, glacier ablation in the Ecuadorian Andes is extremely variable. Analysis of the energy balance variables at the surface of Antizana Glacier 15 (0°28′S, 78°09′W, Ecuador) allows better understanding of the involved melting processes. The cycle studied here verifies the absence of temperature and humidity seasonality, which is characteristic of the low latitudes.

[55] The wind demonstrates more pronounced variations. More intense easterly winds blew between 1 June and 15 October 2002, which produced a strong convection and a notable loss of energy through sublimation. However, the variations in the energy balance depend for the most part on albedo values. Snowfall causes a reduction in melting; a halt in melting is only durable when heavy snowfalls occur. Consequently, the net short-wave radiation is the first source of surface energy (123 W m^{-2}). In nearly permanently stable conditions, the sensible heat flux H accounts for 21 W m^{-2}. H counters the heat sink through sublimation: $LE = -27$ W m^{-2}. The main heat sink remains the long-wave radiation balance $L = -39$ W m^{-2}. The entirety of turbulent fluxes only consume 7% of the all-wave net radiation contribution. This heat sink cannot be ignored between 1 June and 15 October 2002 (21% of the values of R for the period) and the turbulent fluxes therefore play an important role in decelerating the melting processes. The

incident potential radiative flux is nearly constant throughout the year and the net radiation depends entirely on snowfall. When temperature does not vary and there is no pronounced dry season, rainfalls can occur reaching the equilibrium line throughout the year. By controlling their phase, air temperature during these precipitations is a key variable controlling albedo variables. The 0°C-level intersection with the ablation zone and the snow line positions on the ablation zone determine the close relation between melting and local climate variability.

[56] **Acknowledgments.** The glaciological program is supported by l'Institut de Recherche pour le Développement (IRD, ex-ORSTOM). We are grateful for the assistance received from INAMHI (Instituto Nacional de Meteorologia e Hidrologia) and from EMAAP-Q (Empresa Municipal de Alcantarillado y de Agua Potable de Quito) in Quito. We thank L. Northrup for the correction of the English version of this paper. The important field work done by P. Tachker, E. Praderio, R. Bucher, M. Menegoz and B. Caceres was highly appreciated.

References

Ambach, W. (1974), The influence of cloudiness on the net radiation balance of a snow surface with high albedo, *J. Glaciol.*, *13*(67), 73–84.

Ambach, W. (1986), Nomographs for the determination of meltwater from snow and ice surfaces, *Ber. Naturwiss. Med. Ver. Innsbruck*, *73*, 7–15.

Andreas, E. L. (1987), A theory for scalar roughness and the scalar transfer coefficient over snow and sea ice, *Boundary Layer Meteorol.*, *38*, 159–184.

Arck, M., and D. Scherer (2002), Problems in the determination of sensible heat flux over snow, *Geograf. Ann. A*, *84*(3/4), 157–169.

Barry, R. G. (1992), *Mountain Weather and Climate*, 1st ed., 400 pp., Routledge, New York.

Bintanja, R., S. Jonsson, and W. Knap (1997), The annual cycle of the surface energy balance of Antartic blue ice, *J. Geophys. Res.*, *102*(D2), 1867–1881.

Bourges, B. (1985), Improvement in solar declination computation, *Sol. Energy*, *35*(4), 367–369.

Brun, E., E. Martin, V. Simon, C. Gendre, and C. Coleou (1989), An energy and mass model of snow cover suitable for operational avalanche forecasting, *J. Glaciol.*, *35*(121), 333–342.

Brun, E., P. David, M. Sudul, and G. Brunot (1992), A numerical model to simulate snow-cover stratigraphy for operational avalanche forecasting, *J. Glaciol.*, *38*(128), 13–22.

Brutsaert, B. (1982), *Evaporation in the Atmosphere, Theory, History, and Applications*, 299 pp., Kluwer Acad., Norwell, Mass.

De la Casinière, A. C. (1974), Heat exchange over a melting snow surface, *J. Glaciol.*, *13*(67), 55–72.

Denby, B., and W. Greuell (2000), The use of bulk and profile methods for determining surface heat fluxes in the presence of glacier winds, *J. Glaciol.*, *46*(154), 445–452.

Diaz, H. F., and N. E. Graham (1996), Recent changes in tropical freezing heights and the role of sea surface temperature, *Nature*, *383*, 152–155.

Francou, B., E. Ramírez, B. Cáceres, and J. Mendoza (2000), Glacier evolution in the tropical Andes during the last decades of the 20th century: Chacaltaya, Bolivia, and Antizana, Ecuador, *Ambio*, *29*, 416–422.

Francou, B., M. Vuille, P. Wagnon, J. Mendoza, and J. E. Sicart (2003), Tropical climate change recorded by a glacier in the central Andes during the last decades of the 20th century: Chacaltaya, Bolivia, 16°S, *J. Geophys. Res.*, *108*(D5), 4154, doi:10.1029/2002JD002959.

Francou, B., M. Vuille, V. Favier, and B. Cáceres (2004), New evidence for an ENSO impact on low-latitude glaciers: Antizana 15, Andes of Ecuador, 0°28′S, *J. Geophys. Res.*, *109*, D18106, doi:10.1029/2003JD004484.

Gaffen, D. J., B. D. Santer, J. S. Boyle, J. R. Christy, N. E. Graham, and R. J. Ross (2000), Multidecadal changes in the vertical temperature structure of the tropical troposphere, *Science*, *287*, 1242–1245.

Halberstam, I., and J. P. Schieldge (1981), Anomalous behaviour of the atmospheric surface layer over a melting snowpack, *J. Appl. Meteorol.*, *20*, 255–265.

Hastenrath, S. (1978), Heat-budget on the Quelccaya ice cap, Peruvian Andes, *J. Glaciol.*, *20*(82), 85–97.

Hastenrath, S. (1981), *The Glaciation of the Ecuadorian Andes*, 173 pp., A. A. Balkema, Brookfield, Vt.

Hastenrath, S. (1991), *Climate Dynamics of the Tropics*, 488 pp., Kluwer Acad., Norwell, Mass.

Hastenrath, S., and P. D. Kruss (1992), The dramatic retreat of Mount Kenya's glaciers between 1963 and 1987: Greenhouse forcing, *Ann. Glaciol.*, *16*, 127–133.

Hock, R. (1998), Modelling of glacier melt and discharge, Ph.D. thesis, 126 pp., ETH Geograph. Inst., ETH Zürich, Zurich, Switzerland.

Hock, R., and B. Holmgren (1996), Some aspects of energy balance and ablation of Storglaciären, northern Sweden, *Geograf. Ann. A*, *78*, 121–131.

Kaser, G. (2001), Glacier-climate interaction at low-latitudes, *J. Glaciol.*, *47*(157), 195–204.

Kaser, G., and H. A. Osmaston (2002), *Tropical Glaciers*, 228 pp., Cambridge Univ. Press, New York.

Kaser, G., M. Ames, and M. Zamora (1990), Glacier fluctuation and climate in the Cordillera Blanca, Peru, *Ann. Glaciol.*, *14*, 136–141.

King, J. C., and P. S. Anderson (1994), Heat and water vapour fluxes and scalar roughness lengths over an Antartic Ice Shelf, *Boundary Layer Meteorol.*, *69*, 101–121.

Klok, E. J., and J. Oerlemans (2002), Model study of the spatial distribution of the energy and mass balance of Morteratschgletscher, Switzerland, *J. Glaciol.*, *48*(163), 505–518.

Kuhn, M. (1981), Climate and glaciers, in *Sea Level, Ice and Climatic Change (Proceedings of the Canberra Symposium)*, *IAHS Publ.*, *131*, 3–20.

Male, D. H., and R. J. Granger (1981), Snow surface energy exchange, *Water Resour. Res.*, *17*(3), 609–627.

Marks, D., and J. Dozier (1992), Climate and energy exchange at the snow surface in the alpine region of the Sierra Nevada: 2. Snow cover energy balance, *Water Resour. Res.*, *28*(11), 3043–3054.

Martin, S. (1975), Wind regimes and heat exchange on glacier De Saint-Sorlin, *J. Glaciol.*, *14*(70), 91–105.

Meesters, A. G. C. A., N. J. Bink, H. F. Vugts, F. Cannemeijer, and E. A. C. Henneken (1997), Turbulence observations above a smooth melting surface on the Greenland Ice Sheet, *Boundary Layer Meteorol.*, *85*, 81–110.

Michaux, H. (1928), *Equador: Journal De Voyage*, 188 pp., Ed. Gallimard, Paris.

Mölg, T., D. R. Hardy, and G. Kaser (2003), Solar-radiation-maintained glacier recession on Kilimanjaro drawn from combined ice-radiation geometry modeling, *J. Geophys. Res.*, *108*(D23), 4731, doi:10.1029/2003JD003546.

Moore, R. D. (1983), On the use of bulk aerodynamic formulae over melting snow, *Nord. Hydrol.*, *14*(4), 193–206.

Morris, E. M. (1989), Turbulent transfer over snow and ice, *J. Hydrol.*, *105*, 205–223.

Munro, D. S. (1989), Surface roughness and bulk heat transfer on a glacier: Comparison with eddy correlation, *J. Glaciol.*, *35*(121), 343–348.

Obleitner, F., and J. de Wolde (1999), On intercomparison of instruments used within the Vatnajökull glacio-meteorological experiment, *Boundary Layer Meteorol.*, *92*, 27–37.

Oerlemans, J. (1998), The atmospheric boundary layer over melting glaciers, in *Clear and Cloudy Boundary Layer*, edited by A. A. M. Holtslag and P. G. Duynkerke, pp. 129–153, R. Netherlands Acad. of Arts and Sci., Amsterdam.

Oerlemans, J. (2001), *Glaciers and Climate Change*, 148 pp., A. A. Balkema, Norwell, Mass.

Oerlemans, J., and B. Grisogono (2002), Glacier winds and parameterisation of the related surface heat fluxes, *Tellus*, *Ser. A*, *54*, 440–452.

Oerlemans, J., and E. J. Klok (2002), Energy balance of a glacier surface: Analysis of AWS data from the Morteratschglatscher, Switzerland, *Arct. Antarct. Alp. Res.*, *34*(123), 115–123.

Oerlemans, J., and W. Knap (1998), A 1 year record of global radiation and albedo in the ablation zone of Morteratschgletscher, Switzerland, *J. Glaciol.*, *44*(147), 231–238.

Oke, T. R. (1987), *Boundary Layer Climates*, 2nd ed., 435 pp., Routledge, New York.

Schwerdtfeger, W. (1976), *World Survey of Climatology*, vol. 12, *Climates of Central and South America*, Elsevier Sci., New York.

Sicart, J. E. (2002), Contribution à l'étude des flux d'énergie, du bilan de masse et du débit de fonte d'un glacier tropical: Le Zongo, Bolivie, Ph.D. thesis, 333 pp., Univ. Paris VI, Paris.

Sicart, J. E., P. Ribstein, P. Wagnon, and D. Brunstein (2001), Clear-sky albedo measurements on a sloping glacier surface: A case study in the Bolivian Andes, *J. Geophys. Res.*, *106*(D23), 31,729–31,737.

U.S. Army Corps of Engineers (1956), Summary report of the snow investigations, snow hydrology, North Pac. Div., Portland, Oreg.

Van den Broeke, M. R. (1997), Momentum, heat and moisture budgets of the katabatic wind layer over a mid-latitude glacier in summer, *J. Appl. Meteorol.*, *36*, 763–774.

Vuille, M., and R. S. Bradley (2000), Mean annual temperature trends and their vertical structure in the tropical Andes, *Geophys. Res. Lett.*, *27*(23), 3885–3888.

Vuille, M., R. S. Bradley, and F. Keimig (2000), Climate variability in the Andes of Ecuador and its relation to tropical Pacific and Atlantic sea surface temperature anomalies, *J. Clim.*, *13*, 2520–2535.

Wagnon, P., P. Ribstein, B. Francou, and B. Pouyaud (1999), Annual cycle of energy balance of Zongo Glacier, Cordillera Real, Bolivia, *J. Geophys. Res.*, *104*(D4), 3907–3923.

Wagnon, P., P. Ribstein, B. Francou, and J. E. Sicart (2001), Anomalous heat and mass budget of Zongo Glacier, Bolivia, during the 1997–98 El Niño year, *J. Glaciol.*, *47*(156), 21–28.

Warren, S. G. (1982), Optical properties of snow, *Rev. Geophys.*, *20*(1), 67–89.

J.-P. Chazarin and V. Favier, Maison des Sciences de l'Eau, IRD, BP 64501, 34394 Montpellier Cedex 5, France. (favier@msem.univ-montp2.fr)

A. Coudrain, UMR Hydrosciences, Maison des Sciences de l'Eau, 300 avenue Emile Jeanbrau, 34095 Montpellier Cedex 5, France.

L. Maisincho, INAMHI, Iñaquito y Corea, 16-310 Quito, Ecuador.

P. Wagnon, IRD-LGGE, 54 rue Molière, BP 96, 38402 Saint Martin d'Hères, France.